Sci. Rep. Kanazawa Univ. **ARTICLES**
Vol. 61, pp. 39-47, 2017

Landslide displacement detection around Hakusan volcano, central Japan, from InSAR analysis of ALOS-2/PALSAR-2 data

Yuya KITOH [1,*] and Yoshihiro HIRAMATSU [2]

[1] Graduate School of Natural Science and Technology, Kanazawa University, Kakuma, Kanazawa, 920-1192, Japan
[2] School of Natural System, Institute of Science and Engineering, Kanazawa University, Kakuma, Kanazawa, 920-1192, Japan

(Received December 12, 2017 and accepted in revised form February 5, 2018)

Abstract InSAR analysis using ALOS-2/PALSAR-2 data was conducted to detect landslides around Hakusan volcano, where we observed landslide movements in three areas. In the Jinnosukedani area, we detected landslide movement with maximum annual displacement of 200 mm, which is consistent with that of GNSS observations on the ground surface. In the Yunotani area, we detected landslide movement with maximum annual displacement of 200 mm. The landslide area detected by the InSAR analysis is almost coincident with a previous study of InSAR analysis, although the remarkable landslide area with annual displacement of 100–200 mm is narrower than that reported by the previous study. In the Sennindani area, a large slope collapse can be captured by InSAR analysis as a low coherence area. InSAR analysis around Hakusan volcano provides results that are consistent with those of the ground-based monitoring in the field, indicating that InSAR analysis is a useful landslide-monitoring tool.

Keywords. Interferometric synthetic aperture radar, Jinnosukedani area, Yunotani area, Sennindani area, Landslide movement, Slope collapse, GNSS observation

1 Introduction

Landslides, which are an important factor of geomorphic development because they alter topography, are often induced suddenly by heavy rains, earthquakes, and volcanic eruptions. However, some landslides are unrelated to those events and continue at a constant rate for long durations.

Landslide movements have been monitored using GNSS (Global Navigation Satellite System) and other instruments (e.g. Ueno and Nakazato, 2012). Most methods used to monitor landslides measure the amount of displacement at a selected locality. For that reason, it is difficult to ascertain the spatial distribution of landslides. Synthetic Aperture Radar (SAR) irradiates microwaves from sensors mounted on satellites or aircraft to the Earth's surface and then receives the backward-scattered waves (Hanssen, 2001). Interferometric synthetic aperture radar (InSAR) is a method that estimates ground movement from some SAR data (Massonnet et al., 1998; Bürgmann et al., 2000). Although InSAR analysis was developed initially as a tool to detect surface changes caused by earthquakes and volcanic activities (Massonnet et al., 1993, 1995; Tobita et al., 2001; Ozawa, 2006), its application to other fields has advanced in recent years. Several InSAR-analysis-based studies of landslides have been reported (Une et al., 2008; Sato et al., 2012; Nishiguchi, 2017). Around Hakusan volcano, Michinaka and Hiramatsu (2010)

*Corresponding author E-mail: kitoh@live.jp

reported landslide displacement using ALOS data obtained by the satellite predecessor.

Several SAR satellites are available for InSAR analysis. In May 2014, the Japan Aerospace Exploration Agency (JAXA) launched ALOS-2, which is equipped with SAR of the L band sensor (PALSAR-2). The ALOS-2 produces higher resolution data than past satellites. We expect that analysis of ALOS-2 data can clarify features of landslides better than earlier studies.

This study estimates the area and the annual displacement of landslides around Hakusan volcano from InSAR analysis. By comparing landslides detected using InSAR analysis with ground monitoring results (Kanazawa River National Highway Office, 2015), we evaluate its consistency.

2 Study area and Data set

2.1 Study area

Hakusan volcano, located on the prefectural border of Ishikawa and Gifu in central Japan, is at the center of the study areas (Figure 1). Its surrounding area includes the Tedori group of the Mesozoic Cretaceous, which is covered by Hakusan volcanic ejecta/deposits (Kaseno, 1993). We overlaid a shaded-relief map with the landslide map compiled by National Research Institute for Earth Science and Disaster Resilience (NIED) (NIED, 2001). Many topographical features around Hakusan volcano are related to landslide movements (Figure 1b).

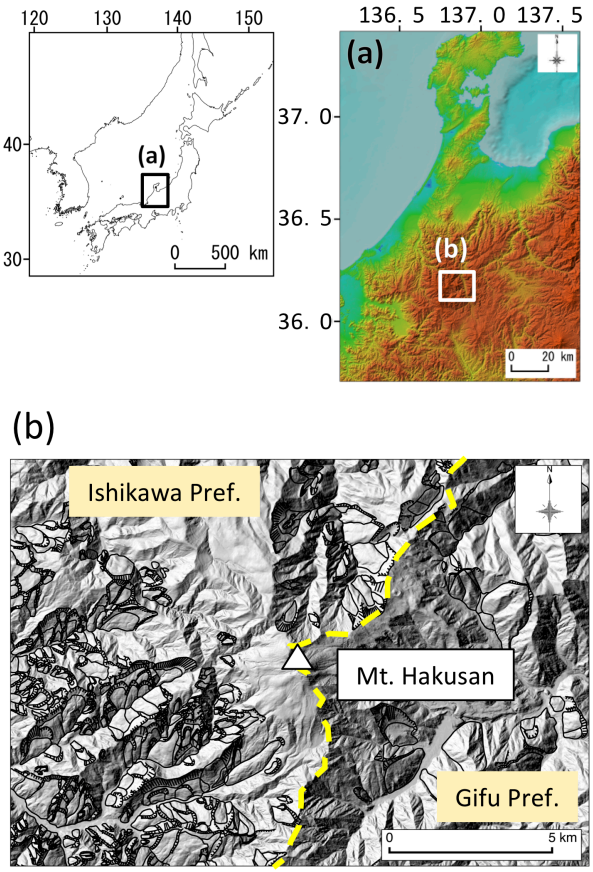

Figure 1. (a) Location and topography in the study area. The white rectangle shows the study area. (b) Shaded relief map of the study area from LiDAR (Light Detection and Ranging) data provided by the Geospatial Information Authority of Japan (GSI). Areas enclosed by black lines are landslide areas reported by the National Research Institute for Earth Science and Disaster Resilience (NIED). Yellow broken line represents prefectural boundary.

2.2 Data set

We used SAR images taken on October 8, 2014 and July 15, 2015 acquired by Phased Array L-band Synthetic Aperture Radar-2 (PALSAR-2; 23.8 cm wavelength) of ALOS-2 (Advanced Land Observing Satellite-2) (Table 1).

All data used for analyses were obtained in high-resolution mode, imaged obliquely downward to the right in ascending (northward) orbit. The pass/frame, which represents the observation area, is 127/710. The satellite advancing direction from the north (the off-nadir azimuth) (α) is 350.5° at the observation time. The incidence angle of the microwave at the scene center (θ) is 42.9°. The perpendicular baseline distance between the satellites at the time of data capture is 215 m (Table 1).

We used GNSS data observed by the Kanazawa River National Highway Office of the Hokuriku Regional Development Bureau of the Ministry of Land, Infrastructure and Transport in the Jinnosukedani area in October 2014 and October 2015.

Table 1. InSAR analysis information.

Master observation date	Slave observation date	Perpendicular baseline (m)
October 8, 2014	July 15, 2015	215

3 Methods

For InSAR analysis, the software used for InSAR analysis was RINC ver. 0.31 (Ozawa, 2014). Phase differences obtained using InSAR analysis are affected not only by ground deformation that is apparent from two datasets but also by satellite orbit conditions, topographic conditions, and atmospheric conditions. JAXA and the Geospatial Information Authority of Japan (GSI) provide precise satellite orbit data and 10 m DEM, respectively. We used these data to correct the respective conditions of a satellite orbit, topography, and atmosphere. Furthermore, we estimated the phase change correlated with the terrain (Ozawa, 2014) and removed this phase change as the effect of the atmosphere. For the calculating the phase change, it is important to reduce the noise attributable to reflection from multiple objects on the ground surface. We applied so-called multi-look processing (Hanssen, 2001), averaging neighboring pixel data to reduce noise. Ozawa (2014) reported that the number of looks depended on a research subject. In this study, we focus landslide movement with the area of several hundred meters. Previous studies often applied 5–10 look processes for landslide movement (e.g. Sato, 2016). For this study, we processed five-look processes in the range and azimuth directions. The spatial resolution of the ground motion diagram of the analysis is about 10 m × 10 m. The interference image filter using the method of Baran et al. (2003) was applied to remove the residual noise. We calculated the displacement along the SAR line of sight (LoS) direction (D_{LoS}) from the phase value using software (SNAPHU; Chen and Zebker, 2002). This procedure, called phase unwrapping, is formulated as

$$D_{LoS} = \lambda \Delta\phi / 4\pi, \quad (1)$$

where λ and $\Delta\phi$ represent the wavelength and the phase difference, respectively. We estimated the landslide displacement from D_{LoS} using a vector-transformed formula (Hanssen, 2001) as

$$D_{LoS} = D_u \cos(\theta) - \sin(\theta)[D_n \cos(\alpha - 3\pi/2) + D_e \sin(\alpha - 3\pi/2)], \quad (2)$$

where D_u, D_n and D_e denote ground deformation components in the up, north, and east directions, respectively, θ stands for the incidence angle, and α signifies the off-nadir azimuth.

We convert the LoS displacement to the along-slope displacement (D_{slope}) as

$$D_{slope} = D_{LoS} / (n_{slope} \cdot n_{LOS}) \quad (3)$$

where n_{slope} is the unit vector of the slope direction (positive in downslope) and n_{LoS} is the unit vector along the LoS direction orientated positively in the satellite-to-ground direction. The both vectors can be written respectively in the East-North-Up reference system as

$$n_{slope} = (\sin A_s \cos\delta, \cos A_s \cos\delta, -\sin\delta), \quad (4)$$

$$n_{LoS} = (\sin A_L \sin\theta, -\cos A_L \sin\theta, -\cos\theta), \quad (5)$$

where A_s is the slope azimuth angle, δ is the slope angle, and A_L is the LoS azimuth angle (AL = alpha +90). In this study, $A_l = 80.5°$ and $\theta = 42.9°$, leading $n_{LOS} = [0.67, -0.11, -0.73]$. We convert the D_{slope} to the horizontal displacement (D_h) as

$$D_h = D_{slope} \cdot \cos\beta. \quad (6)$$

4 Results of InSAR analysis

We present results of the InSAR analysis around Hakusan volcano in Figure 2a. The flight direction of the SAR satellite is southeast to northwest. The irradiation direction of the radar is southwest to northeast. The displacement is expressed as a change of the distance along the LoS (line-of-sight) direction. Negative and positive values signify approaching or moving away from the satellite. Shadow areas against beam directions are masked because the coherence was reduced in the areas (Figure 2b). We overlaid our results on the landslide map by NIED (2001) (Figure 2b). In the previous study using ALOS-PALSAR data, there were color changes that might be related to the atmospheric effect due to vapor. In other words, those color changes might be unrelated to ground movement. However, in this analysis, such color changes are not hardly seen. This can be interpreted that ALOS-2 data clarify features of landslides better than ALOS data. Our results detect displacements of approx. 70 mm approaching the satellite in two areas about 2–3 km southeast of the Hakusan summit. We also observe remarkable color change in an area about 5 km northeast of the Hakusan summit. In this area, we recognize that the coherence is lower than in the surrounding area. The former corresponds to landslide areas, named as the Jinnosukedani area (Kanazawa River National Highway Office, 2011) and the Yunotani area (Ishikawa Forest Office, 2013). The latter is the Sennindani area, where a large sector collapse occurred in May 2015 (Ishikawa Forest Office, 2015). During the analyzed period, no volcanic activity, large earthquake, or heavy rain occurred. Therefore, we consider that the observed displacement and color change reflect landslide movement.

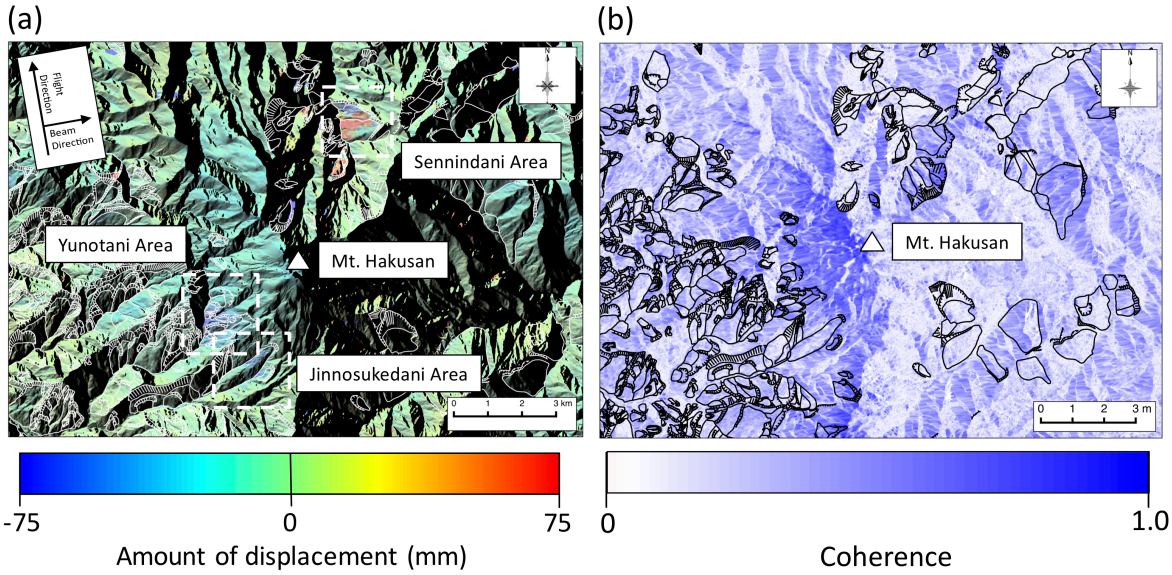

Figure 2. Results of InSAR analysis using PALSAR-2 data around Hakusan volcano overlapped with the landslide area map by NIED (2001). (a) Change in distances between the satellite and the ground estimated from InSAR analysis. Shadow areas against beam directions are masked. (b) Map of coherence.

Figure 3 presents a close-up view of the result of the InSAR analysis around the Jinnosukedani area. In the center of Figure 3, landslide displacements in the range of 400 m × 1000 m are apparent on the upper part of a ridge extending northeast–southwest, called the middle ridge block. Another landslide displacement is apparent in the range of 300 m × 400 m on the southeast slope of another ridge, called the left bank large block. Both displacements are shown as approaching the satellite. The amounts of the displacement in the middle ridge block and in the left bank block are 75 mm and 60 mm (Figure 3), respectively. The area of the landslide around the Jinnosukedani area observed in this study is concordant with previously reported landslide topography (Kanazawa River National Highway Office, 2015). Based on the direction of the slope where the landslide is observed, we infer that the displacement approaching the satellite represents horizontal movement in the dip direction of the slope and uplift of the slope and that the displacement moving away from the satellite represents the slope subsidence. The horizontal displacement in the landslide direction was calculated from the displacement shown in Figure 3 by using vector conversion with the slope angle (δ) and the slope azimuth angle (A_s) reported by Michinaka and Hiramatsu (2010). The middle ridge block has the slope angle (δ) of 20.4° and the slope azimuth angle (A_s) of 223°. The left bank large block has the slope angle (δ) of 28.2° and the slope azimuth (As) of 270°. The annual displacement was calculated proportionally from the displacement for nine months from October 2014 to July 2015. With these values, we estimate the annual horizontal displacement of 200 mm at maximum on the middle ridge block and the annual horizontal displacement of 100 mm at maximum on the left bank large block (Figure 7a).

Figure 4 presents variation of the elevation and

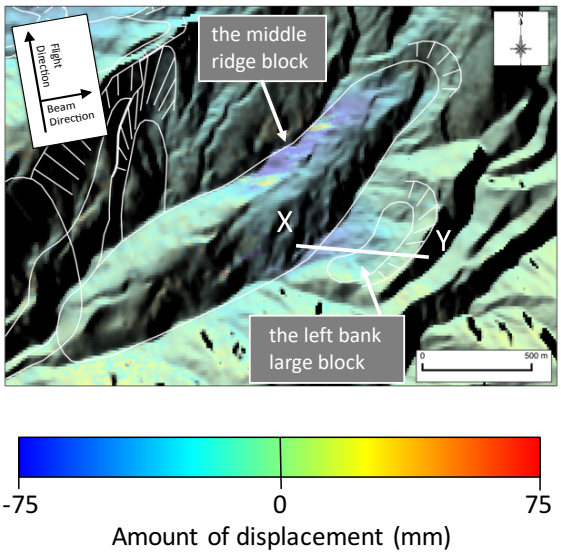

Figure 3. Displacement estimated from InSAR analysis in the Jinnosukedani area. Shadow areas against beam directions are masked.

displacements on the left bank large block along the X–Y line, as depicted in Figure 3. The amounts of horizontal and vertical displacements in Figures 4c and 4d are estimated by converting the change in the distance between the satellite and the ground surface to the values in the slope direction. From Figure 4a and 4b, the change in the distance between the satellite and the ground surface is approximately equal to -50 mm at the distance from 0 m (the lower end of the slope) to 100 m, increases gradually with distance, and reaches 0 m at the upper end of the slope. Generally, landslides cause vertically upward movement at the lower part of a slope and vertically downward movement at the upper part of the slope. Therefore, for a slope facing the satellite, one can expect that both the horizontal and vertical displacements decrease from the lower end to the upper end of the slope. The estimated horizontal and vertical displacements satisfy these features well. The horizontal displacement decreased from 100 mm to 0 mm with distance (elevation) (Fig. 4c). The vertical displacement decreased from 80 mm to 0 mm with distance (elevation) (Figure 4d).

Figure 5 presents results obtained around the Yunotani area. Near the center of Figure 5, one can observe a displacement of 50 mm approaching the satellite in an area of 1000 m × 1000 m. In this area, a large displacement zone, up to 75 mm, is apparent, with spatial scale of 300 m × 500 m.

Figure 6 shows the change in the distances between the satellite and the ground surface and coherence around the Sennindani area. Two remarkable areas of color changes are visible on the northern and southern parts in Figure 6, with the reduction of coherence. For InSAR analysis, it is difficult to perform phase unwrapping if the displacement exceeds a half wavelength of the radar, meaning that it is difficult to detect the ground deformation quantitatively. In Figure 6b, one can recognize that the coherence values are less than 0.1 in the two areas. Therefore, we cannot estimate the displacement correctly in the two areas, although we show the displacement in these areas in Figure 6a as a result of the InSAR analysis. In other words, it is inferred that there might be some large topographic change that InSAR analysis cannot detect correctly in these areas. The sizes of the northern and southern areas with low coherence are 1000 m × 1000 m and 500 m × 500 m, respectively. Both areas are consistent with the landslide area shown in the Hakusan landslide map (NIED, 2001).

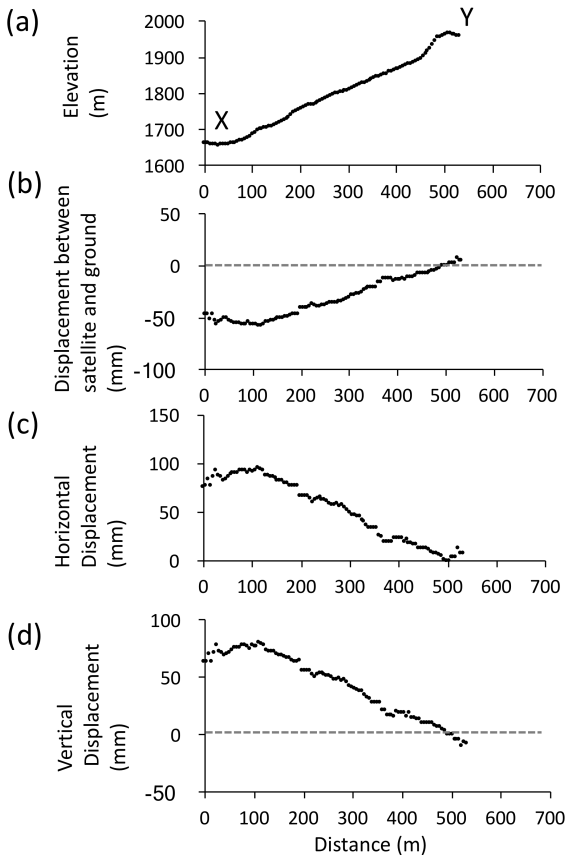

Figure 4. (a) Elevation, (b) displacement between satellite and ground, (c) horizontal displacement, and (d) vertical displacement along the X-Y line (Figure 3) in the Jinnosukedani area.

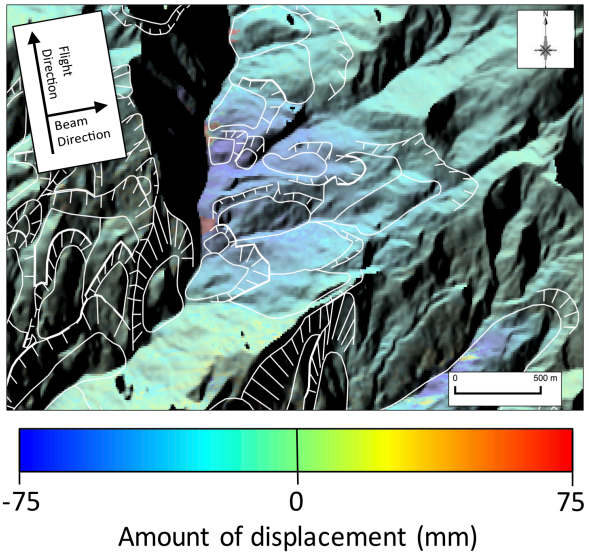

Figure 5. Displacement estimated from InSAR analysis in the Yunotani area. Shadow areas against beam directions are masked.

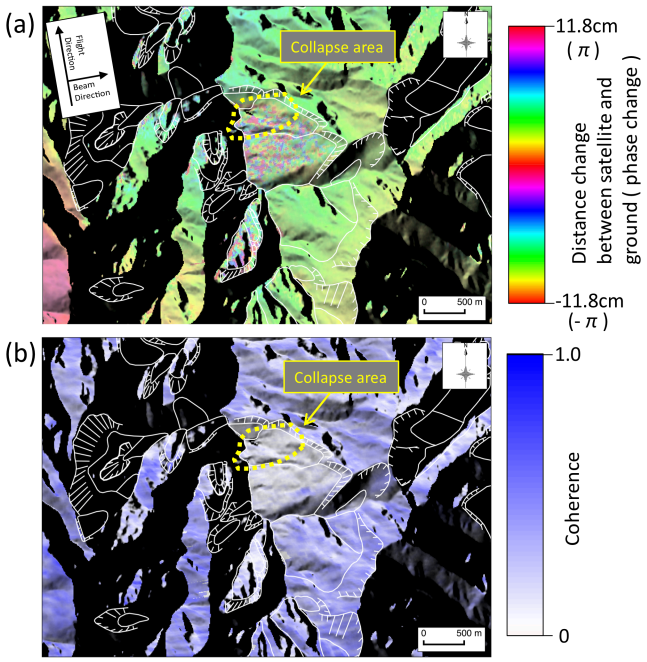

Figure 6. (a) Phase change and (b) coherence of InSAR analysis in the Sennindani area. Shadow areas against beam directions are masked.

5 Discussion

Figure 7a presents results of the GNSS observations on October 2014 and October 2015 (Kanazawa River National Highway Office, 2015), together with our results obtained from InSAR analysis, in the Jinnosukedani area. The GNSS observations show that the horizontal displacements vary from 10 to 220 mm with the measurement locations. Large horizontal displacements from GNSS observations are observed at points on the large displacement areas from InSAR analysis. To compare both results directly, we converted displacements obtained from InSAR analysis into horizontal displacements along the moving direction of the ground estimated from GNSS observations. Horizontal displacements from GNSS observations correlate well with those from the InSAR analysis (Figure 7b). The coefficient of determination is 0.98.

We compare the area and the amount of the landslide in the Jinnosukedani and the Yunotani areas obtained in this study with those reported by

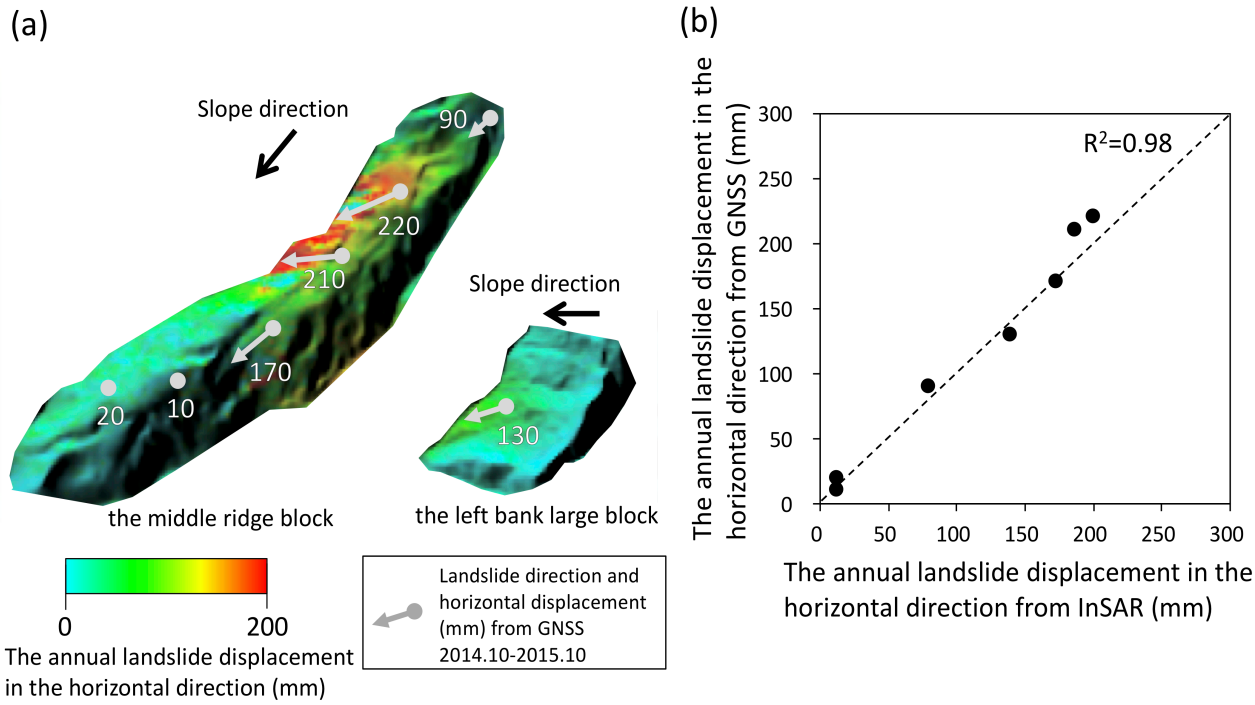

Figure 7. Comparison of displacement estimated from GNSS observations with displacement estimated from InSAR analysis. (a) Gray circles show locations of GNSS observation sites. Displacement estimated from InSAR is converted to horizontal displacement in the direction of the displacement from GNSS observation during October 2014 – October 2015. (b) Plot of the annual horizontal displacement estimated from InSAR analysis versus that from GNSS observation. The coefficient of determination of the plots is 0.98.

Michinaka and Hiramatsu (2010) in Figure 8. In the Yunotani area, the maximum landslide displacement in Figure 5 is 75 mm, which is approaching the satellite. The horizontal displacement in the landslide direction and the annual displacement were calculated as the same way as for the Jinnosukedani area. The slope angle (δ) and the slope azimuth angle (A_s) are 19.1° and 258°, respectively (Michinaka and Hiramatsu, 2010). The areas of the landslide of the two studies are approximately consistent. In the Jinnosukedani area, the area where the annual displacement of the landslide of about 100 mm or less detected in this study is almost consistent with that reported by Michinaka and Hiramatsu (2010). In the Yunotani area, the area of the annual displacement of about 100 mm or less is also consistent between the two studies. However, the remarkable landslide area with annual displacement of about 100–200 mm of this study is narrower than in the previous study. We detect remarkable landslide displacement only in the lower part of the slope. The difference in resolution between the PALSAR data used in the previous study and the PALSAR-2 data used for this study might cause the differences apparent in the landslide areas. Another possible source of the difference in the landslide area is seasonal change of landslides. In general, landslides move greatly during the rainy season and during the snowmelt period, and often show periodicity (e.g. Terzaghi, 1950). The analysis period used by Michinaka and Hiramatsu (2010) was June–October, which corresponds to the snow melting period, through the rainy season, to autumn, when landslide movement is most active. In other words, the annual displacement found their study might be excessive estimates, resulting in a wider landslide area. However, the analytical period of the present study is long (October–July) and does not fully include the snow melting period and the subsequent period, which suggests that the estimated annual landslide displacement might be less than the actual value. Therefore, the estimated annual displacement in the present study is likely to be less than that reported by Michinaka and Hiramatsu (2010). The cause of the difference will be specified with other new data in future works.

In the Sennindani area, a large sector collapse occurred on the northern side of the area in May 2015. The Ishikawa Forest Office (2015) reported that the collapse area was 300 m × 600 m (Figure 6). In Figure 6b, for the analysis area as a whole, the value of coherence is 0.3 or greater. This implies that we can

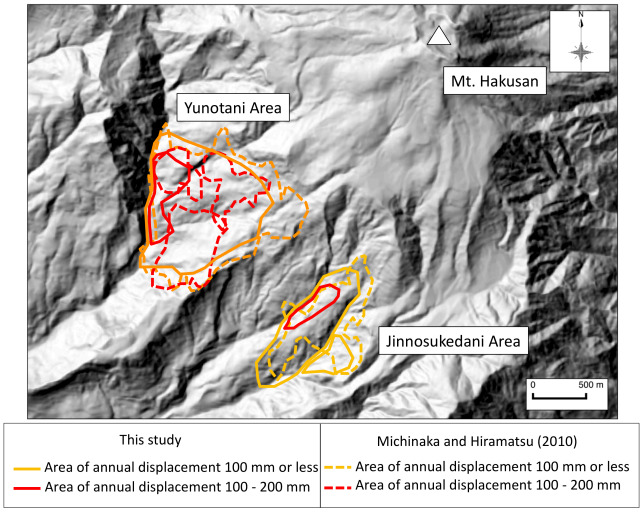

Figure 8. Comparison of landslide areas in this study with those reported by Michinaka and Hiramatsu (2010). Solid orange polygons show areas of displacement about 100 mm/year or less, and dashed ones Michinaka and Hiramatsu (2001). Solid red polygons show the areas of displacement of 100–200 mm, and dashed ones Michinaka and Hiramatsu (2001).

detect landslide movement from InSAR analysis in the Yunotani area. However, the coherence is less than 0.1 in the area of 1000 m × 1000 m on the northern part of Figure 6b. As described previously, low coherence might indicate greater displacement than a half wavelength of the radar. In fact, a remarkable color change is recognized in the area of 1000 m × 1000 m (Figure 6a), which corresponds to low coherence and which includes the collapse area. It is noteworthy that this area is much larger than the collapse area. If this low coherence area reflects landslide movement, then we suggest that the collapse is only a superficial phenomenon. We present the possibility that the landslide occurred in a wider area of the ridge in the northern part of the Sennindani area. Furthermore, Figure 6 suggests the possibility of another landslide in the southern part of the area, where no collapse has been reported, because a remarkable color change and lower coherence are apparent there. Successive monitoring is necessary to clarify features of the landslide in the southern part.

6 Conclusions

From InSAR analysis using ALOS-2/PALSAR-2 data, we detected landslide movements in three areas

(Jinnosukedani area, Yunotani area, and Sennindani area) around Hakusan volcano. The total landslide area in the Jinnosukedani and the Yunotani areas is almost consistent with those reported previously, suggesting continuous landslides there. However, in the Jinnosukedani area, we detected the large landslide movement in a part of the middle ridge block that has not been described in Michinaka and Hiramatsu (2010). In the Yunotani area, the area of displacement found in this study is narrower than that presented in Michinaka and Hiramatsu (2010). The possibility exists of seasonal fluctuation of landslides in these areas, although the data resolutions of the two studies differ. In the Sennindani area, we recognize two low-coherence areas, which implies the possibility of large landslide displacement. One is located in the northern part of the Sennindani area with area of 1000 m × 1000 m, including a collapse area of 300 m × 600 m. The other landslide area, 500 m × 500 m, is located in the southern part in the Sennindani area. These areas are consistent with the landslide area reported previously. There are no remarkable color changes caused by noises in this study, while remarkable color changes caused by noises might be found in Michinaka and Hiramatsu (2010). Therefore, we consider that ALOS-2 data can clarify features of landslides better than ALOS data. The landslide displacement detected by InSAR analysis in the Jinnosukedani area is consistent with the GNSS observations, demonstrating the availability of InSAR analysis as a landslide monitoring tool around Hakusan volcano.

Acknowledgements

This study was supported by the Earthquake Research Institute The University of Tokyo cooperative research program. The PALSAR-2 data are shared by PIXEL and are provided by the Japan Aerospace Exploration Agency (JAXA) through a collaborative research agreement between JAXA and the Earthquake Research Institute (ERI), The University of Tokyo. PALSAR-2 data are owned by the Ministry of Economy, Trade and Industry (METI) and JAXA. We used RINC ver. 0.31 (Ozawa, 2014) for InSAR analysis. The GNSS data are provided by the Kanazawa River National Highway Office of the Hokuriku Regional Development Bureau of the Ministry of Land, Infrastructure and Transport. Constructive comments from two anonymous reviewers are useful to improve the manuscript.

References

[1] Baran, I., Stewart, M.P., Kampes, B.M., Perski, Z., Lilly, P. (2003) A modification to the Goldstein radar interferogram filter. Remote Sens 41:2114–2118. doi: 10.1109/TGRS.2003.817212

[2] Bürgmann, R., Rosen, P.A., Fielding, E.J. (2000) Synthetic aperture radar interferometry to measure Earth's surface topography and its deformation. Annu Rev Earth Planet Sci 28:169–209

[3] Chen, C.W., Zebker, H.A. (2002) Phase unwrapping for large SAR interferograms : Statistical segmentation and generalized network models. IEEE Trans Geosci Remote Sens 40:1709–1719. doi: 10.1109/TGRS.2002.802453

[4] Hanssen Ramon F (2001) Radar Interferometry: data interpretation and error analysis. Kluwer Academic Publishers, Dordrecht.

[5] Ishikawa Forest Office (2013) Outline of the chisan project in the private forests, Ministry of Agriculture, Forestry and Fisheries Kinki Chugoku Regional Forest Office Ishikawa Forest Office (in Japanese) website. http://www.rinya.maff.go.jp/kinki/tisan/pdf/tedorigawa.pdf

[6] Ishikawa Forest Office (2015) The survey report about the landslide at the Tedori river upstrem, Ministry of Agriculture. Forestry and Fisheries Kinki Chugoku Regional Forest Office Ishikawa Forest Office (in Japanese) website. http://www.rinya.maff.go.jp/kinki/kikaku/pdf/270603_tetori-tyosaketuka.pdf

[7] Kanazawa River National Highway Office (2011) Explanation materials of the revaluation about the landslide project. Ministry of Land, Infrastructure, Transport and Tourism Hokuriku Regional Development Bureau Kanazawa River National Highway Office (in Japanese) website. http://www.hrr.mlit.go.jp/ohokokai/hyouka/hyouka01/h23/h23_4/7.pdf

[8] Kanazawa River National Highway Office (2015) Landslide displacement survey report for Jinnosukedani landslide. Ministry of Land, Infrastructure, Transport and Tourism Hokuriku Regional Development Bureau Kanazawa River National Highway Office. (in Japanese)

[9] Kaseno, Y. (1993) Geology of Ishikawa Prefecture, Japan (with geological maps). Ishikawa Prefecture and Hokuriku Geological Laboratory, Ishikawa. (in Japanese)

[10] Massonnet, D., Briole, P., Arnaud, A. (1995) Deflation of Mount Etna monitored by space borne

radar interferometry. Nature 375:567.

[11] Massonnet, D., Feigl, K.L. (1998) Radar interferometry and its application to changes in the Earth's surface. Reviews of Geophysics 36:441–500.

[12] Massonnet, D., Rossi, M., Carmona, C., Adragna, F., Peltzer, G., Feigl, K., Rabaute, T. (1993) The displacement field of the Landers earthquake mapped by radar interferometry. Nature 364:138–142.

[13] Michinaka, H., Hiramatsu, Y. (2010) Detection of landslide displacement at Hakusan volcano from interferometric analysis of ALOS/PALSAR data. Journal of the Geodetic Society of Japan 56:179–194. (in Japanese with English abstract)

[14] National Research Institute for Earth Science and Disaster Resilience (NIED) (2001) Research Material No. 210 1 / 50,000 landslide topography map 12th collection "Kanazawa / Nanao / Wajima" website. http://dil-opac.bosai.go.jp/publication/nied_tech_note/landslidemap/pdf-12.html

[15] Nishiguchi, T., Tsuchiya, S., Imaizumi, F. (2017) Detection and accuracy of landslide movement by InSAR analysis using PALSAR-2 data. Landslides 1–8. doi: 10.1007/s10346-017-0821-z

[16] Ozawa, T. (2006) Detection of crustal deformation due to earthquake and volcanic activity using space borne SAR Interferometry. Journal of the Geodetic Society of Japan 52:253–264. (in Japanese with English abstract)

[17] Ozawa, T. (2014) Development of InSAR processing tools in NIED Part 3. Proceedings of Japan Geoscience Union meeting 2014 STT59-P12 website. http://www2.jpgu.org/meeting/2014/session/S-TT59_e.html. Accessed 5 December 2017 (in Japanese)

[18] QGIS Team (2015) QGIS geographic information system. Open Source Geospatial Foundation Project. website. http://www.qgis.org/ja/site/index.html

[19] Sato, H., Okatani, T., Koarai, M., Suzuki, A., Tobita, M., Tarai, H., Sekiguchi, T. (2012) Study of detection of landslide-induced surface deformation using SAR interferograms – Case study in Mt. Gassan area, Yamagata Pref., Japan –. Journal of the Japan Landslide Society 49:61–67. (in Japanese with English abstract)

[20] Sato, H. P., Une, H. (2016) Detection of the 2015 Gorkha earthquake-induced landslide surface deformation in Kathmandu using InSAR images from PALSAR-2 data. Earth, Planets and Space. 68:47.

[21] Terzaghi, K. (1950) Mechanism of Landslides: In Application of Geology to Engineering Practice. Geological Society of America, New York, 83–123.

[22] Tobita, M., Murakami, M., Nakagawa, H., Yarai, H., Fujiwara, S., Rosen, P.A. (2001) 3-D surface deformation of the 2000 Usu Eruption measured by matching of SAR images. Geophys Res Lett 28:4291–4294.

[23] Ueno, S., Nakazato, H. (2012) The progress and the foresight of landslide investigation and observation methods. Journal of the Japan Landslide Society 49:1–11. (in Japanese with English abstract)

[24] Une, H., Sato, H., Yarai, H., Tobita, M. (2008) Analysis of surface deformation induced by the Noto Hanto and the Chuetsu-oki Earthquakes in 2007 using synthetic aperture radar interferograms. Journal of Japan Landslide Society 45:125–131. (in Japanese with English abstract)